PROCEEDINGS OF SCIENCE

Search for anisotropies in the arrival directions of cosmic rays above 32 EeV from Phase One of the Pierre Auger Observatory

Claudio Galelli[a,*] **for the Pierre Auger Collaboration** [*b]

[a] *Università degli studi di Milano, INFN Milano*
via Celoria 16, 20133 Milano, Italy
[b] *Observatorio Pierre Auger,*
Av. San Martín Norte 304, 5613 Malargüe, Argentina

E-mail: spokespersons@auger.org

The toe of the spectrum of ultra-high energy cosmic rays (UHECRs), above ≈50 EeV, is an extremely interesting region for studying the origins of CRs. The potentially small magnetic deflections at these energies are coupled with the presence of the flux suppression, which could be a signature of the maximum acceleration potential of the sources, or could find its explanation in the interactions of cosmic rays with background photons, effectively limiting the region of interest in the search for UHECR sources to a relatively small bubble around us. In this talk we present the latest anisotropy searches carried out by the Pierre Auger Collaboration in the energy range above 32 EeV. The dataset used is that collected in the *phase one* of the Observatory between 2004 and 2020, before the AugerPrime upgrade, for a cumulative exposure of 120000 km^2 sr yr. We have conducted both blind, model-independent searches for overdensities, correlation analyses with astrophysical structures, and cross-correlation studies with catalogs of candidate sources. We have found evidence for a deviation from isotropy at an angular scale of 25 degrees at the 4σ level for UHECRs with energy above 38 EeV.

**** 27th European Cosmic Ray Symposium - ECRS ****
**** 25-29 July 2022 ****
**** Nijmegen, the Netherlands ****

*Full author list: https://auger.org/archive/authors_2022_07.html
*Speaker

PoS(ECRS)017

1. Introduction

The origin of ultra-high energy cosmic rays (UHECRs), the most energetic particles known in the universe reaching above the EeV (10^{18} eV) and up to more than 100 EeV, is elusive and challenging to investigate. Since particles at these energies are charged, the magnetic fields that permeate galactic and extra-galactic space influence and modify the trajectories connecting us and the accelerating regions, thus erasing some of the meaning in the directional information [1]. As these magnetic fields are not yet modeled in a complete way and the charge of each particle is not known in a event-by-event basis, directly correcting the observed arrival direction is not feasible. However, in the so-called *instep* and *toe* region of the cosmic ray spectrum at and above a few tens of EeV, the magnetic deflections could be small enough to retain information on the position of the sources. This is especially true for particles of small enough charge, like protons [2].
Furthermore, at these energies cosmic rays do not travel unobstructed in the universe, but are instead expected to lose energy due to interactions with cosmological backgrounds. In particular, protons undergo photopion production, the so-called *Greisen-Zatsepin-Kuzmin effect* [3][4], while heavier nuclei experience photodissociation interactions. Depending on mass and energy then the mean free path for cosmic rays varies, ranging from around 5 Mpc to 200-300 Mpc. This horizon limits to the local universe the volume to be searched for sources of UHECRs.
The sources have also to be extra-galactic in nature in this energy range: the data collected by the Pierre Auger Observatory above 8 EeV has been shown to exhibit a dipolar anisotropy in its distribution of arrival directions [5]. The dipole direction points $\approx 120^{\circ}$ away from the Galactic center and is consistent at the 2σ level with the distribution of local stellar mass as traced by the 2MASS Redshift survey [6], while the anti-dipole direction is consistent at the 1σ level with the position of the local void [7].
We report the results from the latest paper published by the Pierre Auger Collaboration concerning the searches for anisotropies in arrival directions of UHECRs at small and intermediate angular scales [9]. The paper is the final effort of the Collaboration regarding small and medium scale anisotropies in the so-called *phase one* of the Observatory, i.e. the phase of the Observatory from the beginning of data taking and the implementation of the *AugerPrime* upgrade [11]. This near-complete upgrade will bring many improvements, chief among all for arrival direction studies will be a greater event-by-event discriminating power between primary species in the surface detector, which will help by making possible the selection of a *light*, and thus less deflected by magnetic fields, data set of events. As this is not yet possible in *phase one*, the data set used for the paper included only information about energy and arrival directions.

2. The Data set

The Pierre Auger Observatory is located in Argentina, near the city of Malargue in the province of Mendoza [10]. Stable data acquisition started in 2004. The Observatory has a *hybrid* design, comprising a surface detector (SD) and a fluorescence detector (FD). The SD is an array of particle detectors composed of 1600 water-Cherenkov stations distributed on a triangular grid spanning 3000 km^2; secondary particles of the extensive air shower are sampled as they reach the ground, with full efficiency above 4 EeV and a duty cycle close to 100%. The FD is composed of 27 fluorescence

telescopes located at four sites; the telescopes overlook the SD and sample the fluorescence light emitted by the nitrogen atoms in the atmosphere excited by the passage of the particles of the shower, with a duty cycle of ≈10%. The FD enables calorimetric measurements of the primary energy and is used to calibrate the energy reconstructed by the SD.

In the paper we analysed the 2635 events with reconstructed energy greater than 32 EeV recorded by the SD between 2004, January 1, and 2020, December 31, as the end of Auger phase one. The minimum energy chosen is determined by the highest energy bin in the large scale anisotropy searches performed by the Collaboration. Events recorded with the SD are reconstructed in two different ways based on their zenith angle θ: events with $\theta < 60^\circ$ are labelled as *vertical*, while events with θ between 60° and 80° are considered as *inclined*. For vertical events the reconstruction of the arrival direction is performed by fitting the arrival times of the particles in the shower front to a spherical model; for inclined events the shower front model takes into account muon production and propagation. The angular resolution for both samples is better than 1° at these energies. The energy estimation is derived from different observables in the two samples. The reference energy estimator for the verticals is the signal at a distance of 1000 m from the shower core, $S(1000)$, while for the inclined the muon content with respect to a simulated proton shower of energy 10^{19} eV, N_{19}, is taken. Both estimators are corrected to account for the absorption that showers undergo at different zenith angles, with a procedure called the *constant intensity cut*, or CIC, that reframes them to reference showers of θ 38 and 68 degrees for vertical and inclined events respectively. The corrected estimators, S_{38} and N_{68}, are then converted to energies via the calibration obtained from *hybrid* events, i.e. the events that are observed by both the SD and the FD. This procedure gives a systematic uncertainty of ≈7% at the energies of interest.

Vertical events are included in the data set when the SD station with the largest signal in their reconstruction is surrounded by at least four active station (4T5 selection). Additionally events are requested to fulfill the *a posteriori* condition that the reconstructed shower core falls inside an isosceles triangle of active stations (POS condition). Inclined events are selected when the SD station closest to the reconstructed shower core is surrounded by at least five active stations (5T5). These selection conditions are chosen as they ensure that the footprint of the showers are well contained in the array, discarding events that fall on the borders or regions of the SD that have too many non triggered stations; the conditions however are more relaxed when compared with other analyses by the Collaboration, such as the UHECR spectrum reconstruction [12], thanks to the fact that at these extremely high energies the showers have very wide footprints on the ground, with an average of 17.7 triggered stations. All events were also checked manually to ensure a robust reconstruction.

The selection procedure results in 2040 vertical events and 595 inclined events, with a geometrical exposure of 95700 km^2 sr yr for the vertical sample and 26300 km^2 sr yr for the inclined sample. Checking the consistency of the two subsamples, the ratio between the number of vertical and inclined events is 0.292±0.014, while the ratio of the geometrical exposures is 0.278; the two numbers are consistent at a 1σ level. For this reason in the analyses the ratio N_{incl}/N_{vert} is used in place of the ratio of exposures, to keep the results as data-driven as possible. In the highest energy bin considered in the analysis, E>80 EeV, a deficit of inclined events at the 2σ level is observed. A discussion about this deficit can be found in the appendix A of the referenced paper.

A visualization of the flux of UHECRs with energy above 32 EeV in *top-hat* regions of 25 degrees

centered on a `HEALPix` grid of parameter nSide = 64 [13] covering the field of view of the Observatory is visible in figure 1.

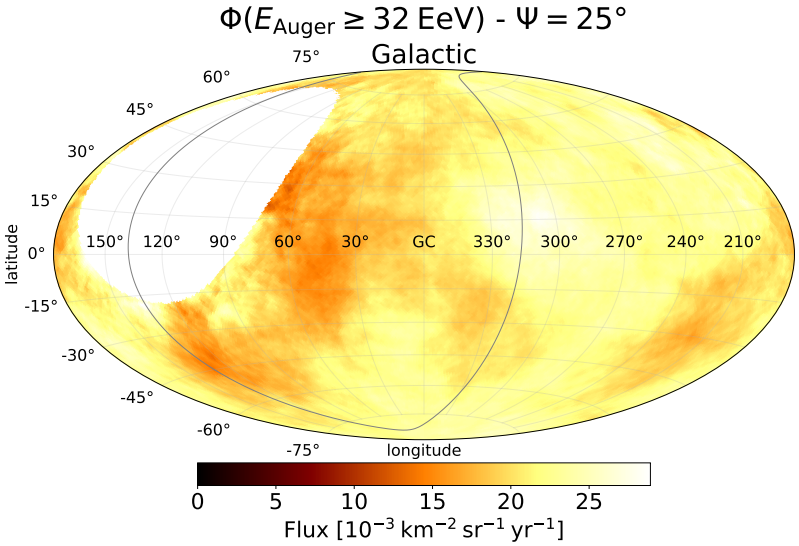

Figure 1: Flux map at energies above 32 EeV and top-hat angle 25° in Galactic coordinates. The supergalactic plane is shown in grey. The blank area indicates the portion of the sky not visible to the Observatory.

3. Searches for overdensities, autocorrelation and correlation with structures

We performed an update of the searches for excesses reported by the Collaboration in an earlier paper published in 2015. Searches for localized excesses in top-hat windows ψ in the whole field of view of the observatory, as well as the autocorrelation analysis, and searches around astrophysical structures of interest such as the Galactic center, Galactic plane and supergalactic plane were performed and repeated above different energy thresholds, from 32 EeV to 80 EeV. The scan is motivated by the limited cosmological horizon from which UHECRs can reach the Earth.

3.1 Blind search for excesses

The first analysis that was performed is a blind search for localized excesses in the portion of the sky in the field of view of the Observatory. This analysis is simple and model-independent, and results in the identification of possible *hotspots* in the data. In this analysis the number of observed events, N_{obs}, taken above an energy threshold E_{th}, within a disk of radius ψ, is compared to the expected number of events from an isotropic distribution of arrival directions, N_{exp}. The search is performed over the entire portion of the sky visible to the Observatory, by centering the search windows on a `HEALPix` grid of parameter nSide = 64. The size of the top-hat disk ψ is scanned from size 1° to 30° in steps of 1 degree; the energy threshold range, from 32 to 80 EeV, is scanned in steps of 1 EeV. N_{exp} is computed from Monte-Carlo simulations of events distributed in right ascension and declination according to the sum of the vertical and inclined relative geometrical exposures at each point, weighted by the observed number of events.

For each point on the sky, each window and threshold energy, we estimated the binomial probability of obtaining N_{obs} or more events by chance from an isotropic distribution of data of mean value N_{exp}. The simulations of isotropic data sets gave us the possibility of taking into account the *look elsewhere effect* occurring by having tested different directions in the sky, threshold energy and sizes for the top-hat disks. We computed the *post-trial* probability as the fraction of simulated data sets with equal or lower local binomial p-value than the observed one. We also computed the local Li-Ma significance [14] for each point in the sky, in which the ψ-sized top-hat disk centered on each pixel of the `HEALPix` grid was considered the ON region and the rest of the field of view the OFF region: the significance map is visible in figure 2.

The most significant excess for this analysis, with 5.4σ local significance, is found at $(\alpha, \delta) = (196.3°, -46.6°)$, at an energy threshold $E_{th} = 41$ EeV and top-hat radius $\psi = 24°$. In this parameter space point, 153 events are observed while 97.7 are expected from isotropy. The local p-value is 3.7×10^{-8}, resulting in a global p-value of 0.03.

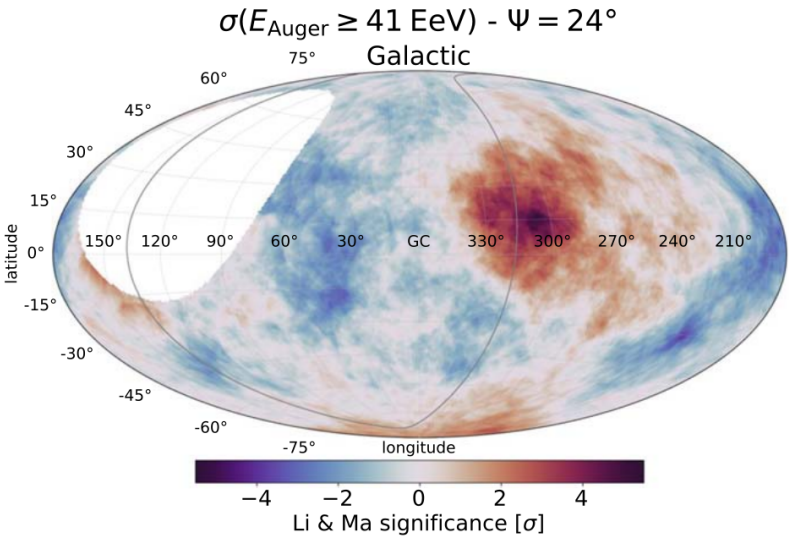

Figure 2: Local Li–Ma significance map at energies above 41 EeV and within a top-hat search angle of $\psi = 24°$ in Galactic coordinates. The supergalactic plane is shown in grey. The white area indicates the portion of the sky not visible to the Observatory.

3.2 Autocorrelation

The search for autocorrelation is the counting of pairs of events separated by a given angular distance. It is another model-independent approach to search for clusters of events and of assessing the typical clustering angular size for a data set. It is a particularly strong analysis in the case of multiple areas in the sky of similar size containing clusters of events.

We report the results of the count of observed event pairs N_{obs}, above energy thresholds ranging from 32 to 80 EeV, with the events in the pair separated by an angular distance ψ; the parameter ψ was scanned from 1° to 30° with steps of 0.25° up to 5°, and steps of 1° above. The distribution of expected number of pairs N_{exp} was obtained by performing the same analysis on simulated isotropic data sets of the same size as the observed one. For each E_{th} and ψ combination, the local p-value was obtained as the fraction of simulated data sets for which $N_{exp} \geq N_{obs}$. The global post-trial

p-value is obtained in the same way as the blind search. The most significant point in parameter space is found at $E_{th} = 62$, $\psi = 3.75°$, where 93 pairs are observed while 66.4 are expected from isotropy, for a local p-value of 2.5×10^{-3} corresponding to a global signficance of 0.24.

3.3 Excesses around astrophysical structures

Results from the searches for large scale anisotropies by the Collaboration decidedly disfavor a Galactic origin for UHECRs with energies above 8 EeV. However, along with the search for an excess in the vicinity of the supergalactic plane, we performed a similar search for the Galactic plane and Galactic center, with the intent of updating previous publications by the Collaboration. The analysis is conducted in a similar way to the previous section, with N_{obs} and N_{exp} in this case being the number of observed and expected events within an angle ψ from the structure. For the Galactic and supergalactic plane this translates into selecting events with latitude smaller than ψ in the respective coordinate system. The most significant excess is found for angles $\psi \geq 20°$ for all three structures. Detailed results are in table 1. No significant departures from isotropy are found.

Search	E_{th} [EeV]	ψ [deg]	N_{obs}	N_{exp}	local p-value	Post-trial
Supergalactic plane	44	20	394	349.1	1.8×10^{-3}	0.13
Galactic plane	58	20	151	129.8	1.4×10^{-2}	0.44
Galactic center	63	18	17	10.1	2.6×10^{-3}	0.57

Table 1: Results for the searches for excesses around astrophysical structures

4. Catalog-based likelihood analysis

In a previous effort by the Collaboration published in 2018, the UHECR arrival directions distribution was cross-correlated via a likelihood-ratio test to four flux-limited catalogs of galaxies. Here we report the results from the updated analysis. The four catalogs that we considered were compiled from observations in different wavelengths: the 2MASS in near infrared, Swift-BAT 105 months in hard X-ray, Fermi-3FHL in γ-rays and Lunardini-19 from the IRAS all-sky, NVSS and Parkes surveys in radio. A brief description of each catalog follows.

As a first more general test, we explored possible correlations with the large scale distribution of matter in the local universe, as traced by the Two Micron All-Sky Survey, 2MASS. The expected UHECR flux in this case may follow K-band observations, which correspond to stellar mass. The catalog used was flux limited to a magnitude of 11.75 in the band of interest. Note that the AGNs present in the sample were kept as part of the catalog, even though their infrared emission comprises a much larger contamination to thermal emission than other classes of galaxies. More than 40000 objects are contained in the final catalog.

Observations in hard X-rays with the Swift-BAT satellite compiled in their 105 months catalog provided a tracer for AGN activity in general [15]. Sources with a flux in the 14-195 keV band larger than 8.4×10^{-12} erg cm^{-2} s^{-1} were selected. All objects identified as AGNs, be they jetted, non-jetted, Seyferts or other species of Active Galaxies, were retained from the sample. We assumed that in this scenario the UHECR luminosity would be driven by accretion onto supermassive black holes, taking the X-ray flux as a direct tracer of the UHECR flux. The final catalog contains 523

galaxies.
A second AGN sample contained only the γ-ray selected galaxies as observed by the Fermi-LAT instrument and tabulated in the 3FHL catalog [16]. We selected radio galaxies and jetted AGNs with integral flux larger than 3.3×10^{-11} cm^{-2} s^{-1} in the 10 GeV - 1 TeV band. In this case the UHECR emission is supposed to be proportional to the γ emission in the jets protruding from the central black hole of the galaxies. The final catalog contains 26 galaxies.
A sample of *starburst* galaxies, i.e. galaxies with a very high star formation rate was distilled from the Lunardini-19 catalog of local objects [17], which already is a synthesis of the IRAS all-sky survey in the far infrared [18], flux limited to objects brighter than 60 Jy at 60 μm, with the NVSS [19] and Parkes [20] surveys in radio, limited to objects brighter than 20 mJy at 1.4 GHz. We further eliminated objects by imposing the ratio between far infrared and radio emission to be between 30 and 1000, eliminating jetted AGNs and dwarf galaxies (in particular the two Magellanic Clouds) respectively. Furthermore, we added the Circinus galaxy, which, being at galactic latitude $-3.8°$, was excluded from the original sample by Lunardini et al. together with all the areas close to the Galactic plane. In this case, UHECR luminosity is thought to be proportional to the star forming rate of the galaxy, giving UHECR emission traced by the measured radio flux. The final catalog contains 44 galaxies.
Precise and robust estimation of the luminosity distance of all the objects in the four catalogs is needed due to the increasing number of interactions that UHECRs suffer by travelling through the cosmological backgrounds; for this reason, all four catalogs were cross-examined with the HyperLEDA database, and the best distance estimate and associated uncertainty was used. All catalogs were cut at 250 Mpc, with exception of the starburst sample which was more conservatively cut at 130 Mpc following the approach of Lunardini et al. The expected flux of UHECR from each galaxy is attenuated with distance to take into account interactions with backgrounds following the best combined-fit model reported by the Pierre Auger Collaboration [21].
We performed an unbinned likelihood ratio test between two hypothesis: pure isotropy versus isotropy with an added component coming from the selected catalog. Both hypothesis were formulated taking into account the exposure of the Observatory. The entity of the contribution of the catalog to the UHECR flux is modeled by the amplitude parameter α, and thus the isotropic portion is $1 - \alpha$. The second free parameter of the analysis is the Fisher-von Mises Gaussian smoothing angle, θ, that is applied to the directions of the objects in the catalogs to obtain the expected flux patterns. Like previous analyses, the energy threshold E_{th} is scanned in the range 32, 80 EeV. As shown in table 2 for all four catalogs the signal is stronger for an energy threshold close to 40 EeV, and equivalent top hat radius $\psi = 1.59\theta$ close to 25°; the signal fraction α ranges form 6 to 15%. Local Test Statistic corresponding to the maximum likelihood ratio for the four catalogs is shown in figure 3. As for previous analyses the local p-values obtained form the TS were penalized for the scan in E_{th} and the two free parameters (α, θ). More details on the calculation of the TS itself and the weighting procedure for the objects in the catalogs can be found in section 4.2 of the reported paper.

The 40 EeV range is the region of the spectrum corresponding to the flux suppression above the toe, which is reported at $E = 46 \pm 3 \pm 6$ EeV by the Pierre Auger Collaboration. The largest deviation from isotropy comes from the starburst galaxy catalog based on radio observations, with a post-trial

Catalog	E_{th} [EeV]	θ [deg]	ψ [deg]	α	TS	Post-trial
All (IR)	40	16	25	16	18.0	7.9×10^{-4}
AGNs (X-rays)	39	16	25	7	19.4	4.2×10^{-4}
jetted AGNs (γ-rays)	39	14	22	6	17.9	8.3×10^{-4}
Starbursts (radio)	38	15	24	9	25.0	3.2×10^{-5}

Table 2: Best fit results obtained with the four catalogs at first maximum. More detail and results for the second maximum in table 2 of the reported paper.

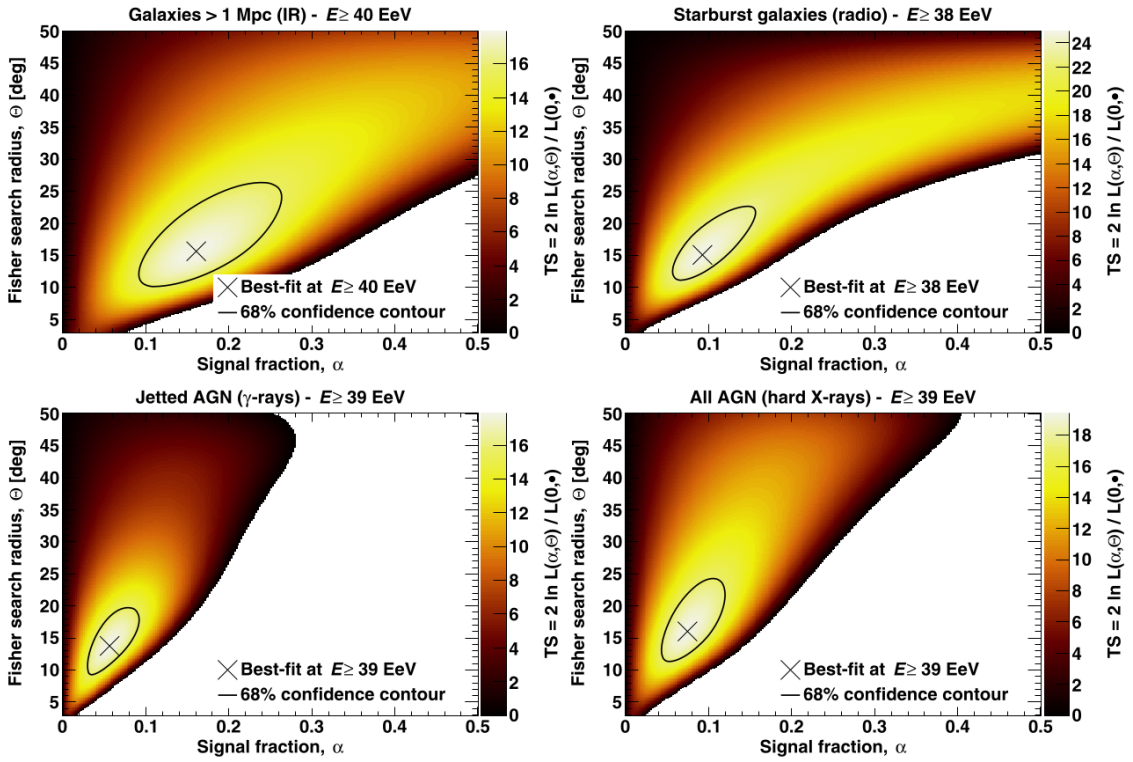

Figure 3: TS as a function of signal fraction and search radius for the four tested catalogs, as labeled in the figure. The reference best-fit parameters obtained above the energy threshold that maximizes the departure from isotropy are marked with a cross. The 68% C.L. contour is displayed as a black line.

p-value of 3.2×10^{-5} corresponding to a 4.0 σ significance. As previously noted, for all catalog the maximum significance is in similar areas of the parameter space. For this reason, we performed a quantitative comparison between the four, by testing composite models with contributions from two different catalogs versus single-catalog models. The results of the best fit flux models are shown in figure 4. The results show models containing a contribution from starburst galaxies are always preferred to the ones excluding them. In all four cases the significance is driven by the contribution of galaxies in the Centaurus region: the flux map obtained both from γ-rays and X-rays is dominated by the jetted AGN CenA, the radiogalaxy and AGN closest to the Milky Way at 3.68 ± 0.05 Mpc; in both cases contributions from other objects is minor (the second contributors in order of importance are respectively Markarian421 for the X-ray catalog and NGC1275 for the γ catalog, both in the rim

of the field of view of Auger). In the case of the starburst catalog the most significant contribution comes from NGC4945 and M83, which are within 20° CenA, with a secondary *warm-spot* close to the galactic south pole dominated by NGC253. This secondary excess is not present in the other flux patterns, and is the main reason for the larger TS of the starburst model. The "all galaxies" model based on IR emission leads to a good reconstruction of the UHECR flux in the Centaurus and Shouthern galactic pole regions, but the significance is lowered by the absence of a *hotspot* in the direction of the Virgo Cluster, which should be the most prominent region due to the massive concentration of close-by galaxies.

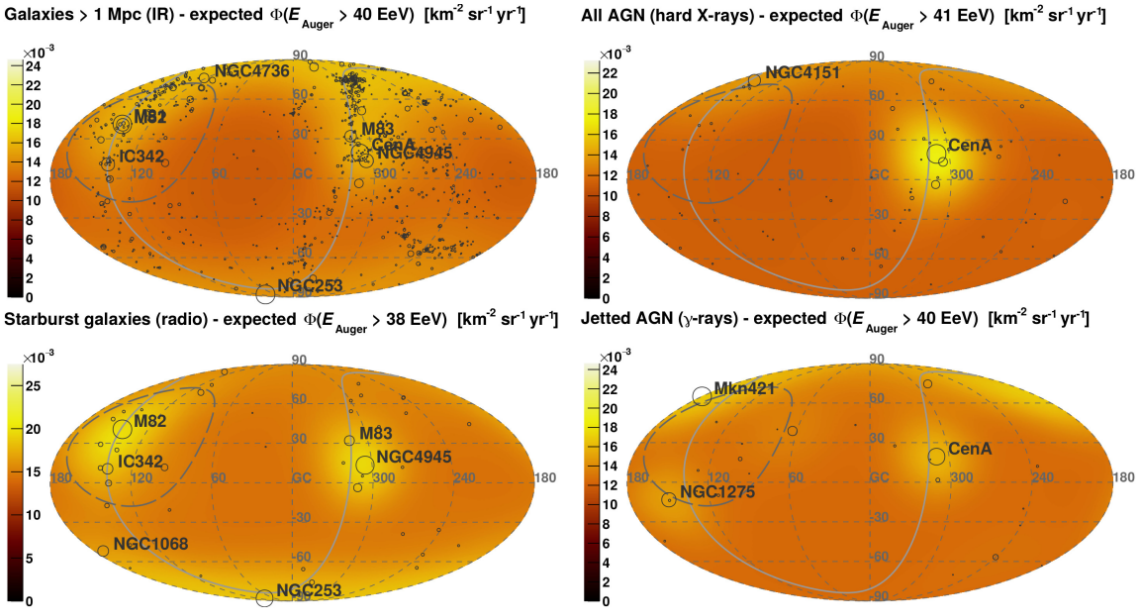

Figure 4: The best-fit flux models of the four catalogs in Galactic coordinates, smoothed on a top-hat scale of 24° as in figure 1. The maps are normalized so that the mean flux in the FoV of the Observatory equals the mean observed flux. The color scales cover the observed flux ranges above the best energy threshold associated to each catalog.

5. The Centaurus region

As noted in the previous section, the region of the sky driving the significance in the likelihood analysis for all four the catalogs, which also roughly corresponds to the position of the most significant excess found by the blind search, is in the direction of a galaxy group colloquially known as the CenA/M83 group. The most prominent members of the group, which lies at a distance of about 4 Mpc, are the radiogalaxy CenA, the Seyfert-starburst galaxy NGC4945 and the starburst M83; they are members of the so-called *Council of Giants* [22], a series of galaxies surrounding the Local Group distributed along the supergalactic plane.

CenA has been the object of previous searches for excesses by the Pierre Auger Collaboration, even since the earliest days of the Observatory [23]. We updated this searches, performing the same analysis described in section 3, but using the position of CenA, $(\alpha, \delta) = (201.4°, -43.0°)$. The map of the local p-values as a function of energy threshold and top-hat search angle is shown in

figure 5. The most significant excess is found at $E_{th} = 38$ EeV, $\psi = 27°$, with a count $N_{obs} = 215$ corresponding to 63 events over $N_{exp} = 152.0$ expected from isotropy. The minimum local p-value, estimated from the binomial probability as in the blind search, is 2.1×10^{-7}, which corresponds to a post-trial p-value of 4.5×10^{-5}. A more in-depth discussion of this result and comparisons to the catalog-based searches can be found in section 5 of the reported paper.

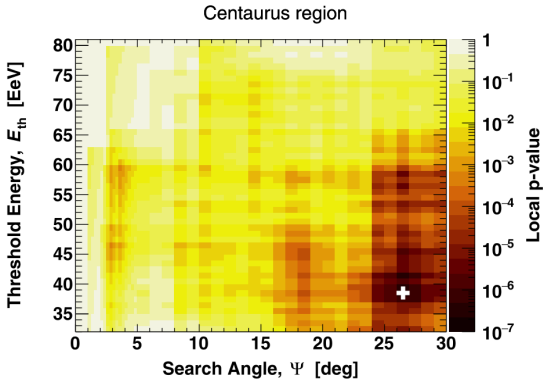

Figure 5: Local p-value for the Centaurus region search as a function of top-hat radius and energy threshold. The minimum p-value location in parameter space is signalled by the white cross

6. Conclusions

In this contribution we have presented the results obtained in the latest paper published by the Pierre Auger Collaboration regarding the searches for anisotropies at small and intermediate angular scales. The data set used is the largest ever created at the extreme energy boundary, thanks to the huge exposure of more than 120000 km^2 sr yr accumulated by the Observatory in the 17 years of operation that make up Auger *phase one*. Although the analyses did not reach discovery significance at 5 σ, evidence for anisotropy at the $\approx 25°$ top-hat angular scale is found in the data, revealing in particular a 4σ correlation signal with a catalog of galaxies with large star formation rate, driven primarily by an excess of events in the Centaurus region and a secondary tepid spot close to NGC253.
The TS for the likelihood analysis and the excess found in the localized search around CenA, if they are indeed a real signal, are expected to grow linearly with the accumulated exposure. This is well reflected by the curves shown in the left panel of figure 6. Fluctuations found around the expected linear behavior are consistent with simulations, shown in the right panels of figure 6. Making predictions from this behavior, a 1-sided 5σ confidence level is expected from the model-independent search around CenA for an accumulated exposure of 165000 km^2 sr yr, reachable in 2025.

Two very important future steps for the identification of the sources of UHECRs are the modeling of the Galactic and extragalactic magnetic fields, and the inclusion of composition-sensitive variables. The latter is one of the main goals of the AugerPrime upgrade, currently in the late stages of deployment, which will open the possibility of using mass-discriminated datasets for arrival direction studies. A second interesting seed of thought is found in the connections, in the

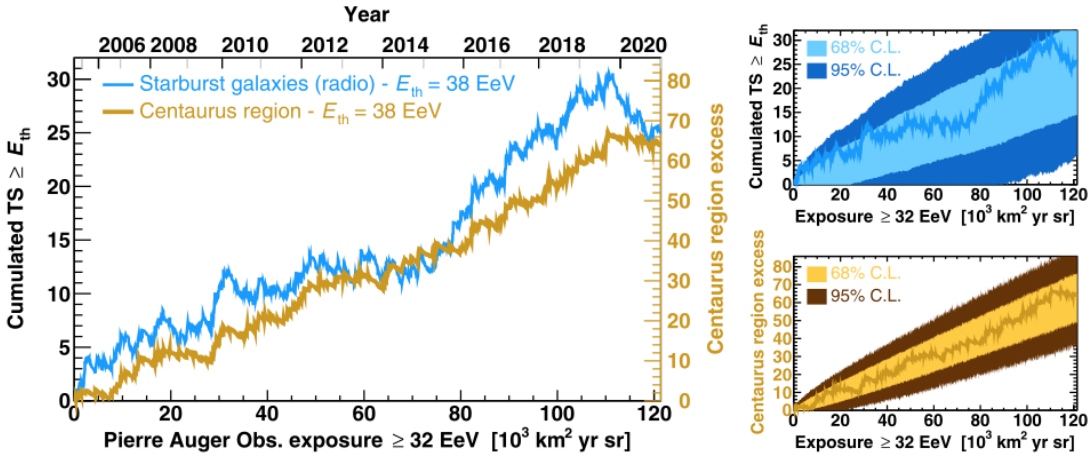

Figure 6: TS of the starburst model and excess in the Centaurus region above the best energy threshold as a function of exposure accumulated by the Pierre Auger Observatory. The fluctuations around the expected linear behavior are consistent with those expected from signal simulations, as illustrated in the right-most panels.

energy range of the *instep*, between the large scale dipolar pattern and the small and intermediate scales. This will be the focus of future publications from the Collaboration.

References

[1] Alves Batista, R., Biteau J., Bustamante M. et al., *Open Questions in Cosmic-Ray Research at Ultrahigh Energies*, 2019, FrASS, 6, 23, doi:10.3389/fspas.2019.00023.

[2] Farrar, G. R., Sutherland, M. S., *Deflections of UHECRs in the Galactic magnetic field*, 2019, JCAP, 2019, 004, doi:10.1088/1475-7516/2019/05/004

[3] Greisen, K., *End to the Cosmic-Ray Spectrum?*, 1966, Phys. Rev. Lett., 16, 748, doi:10.1103/PhysRevLett.16.748.

[4] Zatsepin, G.T. Kuz'min, V.A., *Upper Limit of the Spectrum of Cosmic Rays*, 1966, J. Exp. Theor. Phys. Lett., 4, 78.

[5] The Pierre Auger Collaboration, *Observation of a large-scale anisotropy in the arrival directions of cosmic rays above* 8×10^{18} *eV*, 2017, Science, 357, 1266, doi:10.1126/science.aan4338.

[6] Huchra, J. P., Macri, L. M., Masters, K. L., et al., *The 2MASS Redshift Survey - description and data release*, 2012, ApJS, 199, 26, doi:10.1088/0067-0049/199/2/26

[7] Biteau, J., *Stellar Mass and Star Formation Rate within a Billion Light-years*, 2021, ApJS, 256, 15, doi:10.3847/1538-4365/

[8] The Pierre Auger Collaboration, *Arrival Directions of Cosmic Rays above 32 EeV from Phase One of the Pierre Auger Observatory* 2022 ApJ 935 170, doi:10.3847/1538-4357/ac7d4e

[9] The Pierre Auger Collaboration *An Indication of Anisotropy in Arrival Directions of Ultra-high-energy Cosmic Rays through Comparison to the Flux Pattern of Extragalactic Gamma-Ray Sources*, 2018, Astrophys. J. Lett. 853 L29, doi:10.3847/2041-8213/aaa66d.

[10] The Pierre Auger Collaboration, *The Pierre Auger Cosmic Ray Observatory*, 2015, Nucl. Instrum. Meth. A 798 172, doi:10.1016/j.nima.2015.06.058.

[11] The Pierre Auger Collaboration, *The Pierre Auger Observatory Upgrade - Preliminary Design Report* 2016, arXiv:1604.03637

[12] The Pierre Auger Collaboration, *Measurement of the cosmic-ray energy spectrum above* 2.5×10^{18} *eV using the Pierre Auger Observatory*, 2020, PhRvD, 102, 062005, doi:10.1103/PhysRevD.102.062005

[13] Górski, K. M., Hivon, E., Banday, A. J., et al. *HEALPix: A Framework for High-Resolution Discretization and Fast Analysis of Data Distributed on the Sphere* 2005, ApJ, 622, 759, doi:10.1086/427976

[14] Li, T. P., Ma Y. Q., *Analysis methods for results in gamma-ray astronomy.*, 1983, ApJ 272 317, doi:10.1086/161295

[15] Oh, K., Koss, M., Markwardt, C. B. et al., *The 105-Month Swift-BAT All-sky Hard X-Ray Survey*, 2018, Astrophys. J., Suppl.Ser. 235 4, doi:10.3847/1538-4365/aaa7fd.

[16] The Fermi-LAT Collaboration, Ajello, M. et al., *3FHL: The Third Catalog of Hard Fermi-LAT Sources*, 2017, Astrophys. J., Suppl.Ser. 232 18, doi:10.3847/1538-4365/aa8221.

[17] Lunardini, C., Vance, G. S., Emig, K. L., Windhorst, R. A., *Are starburst galaxies a common source of high energy neutrinos and cosmic rays?*, 2019, J. Cosmol. Astropart. Phys. 10 073, doi:10.1088/1475-7516/2019/10/073.

[18] Sanders, D. B., Mazzarella, J. M., Kim, D. C., Surace, J. A., Soifer, B. T., *The IRAS Revised Bright Galaxy Sample*, 2003, AJ, 126, 1607, doi:10.1086/376841

[19] Condon, J. J., Cotton, W. D., Greisen, E. W., et al., *The NRAO VLA Sky Survey*, 1998, AJ, 115, 1693, doi:10.1086/300337

[20] Calabretta, M. R., Staveley-Smith, L., Barnes, D. G., *A New 1.4 GHz Radio Continuum Map of the Sky South of Declination +25°*, 2014, PASA, 31, e007, doi:10.1017/pasa.2013.36

[21] Guido, E. for the Pierre Auger Collaboration, *Combined fit of the energy spectrum and mass composition across the ankle with the data measured at the Pierre Auger Observatory*, 2021, Proc. 37th Int. Cosmic Ray Conf., online.

[22] McCall, M. L., *A Council of Giants* 2014, MNRAS, 440, 405, doi:10.1093/mnras/stu199

[23] The Pierre Auger Collaboration, *Correlation of the Highest-Energy Cosmic Rays with Nearby Extragalactic Objects* 2007, Sci, 318, 938, doi:10.1126/science.1151124